Electronic Supplementary Information

Experimental Section

Materials: Ammonium chloride (NH_4Cl), sodium hypochlorite solution (NaClO), p-dimethylaminobenzaldehyde ($C_9H_{11}NO$), and sodium nitroferricyanide dihydrate ($C_5FeN_6Na_2O{\cdot}2H_2O$) were purchased from Aladdin Co., Ltd. (Shanghai, China). Hydrochloric acid (HCl), sulfuric acid (H_2SO_4), hydrogen peroxide (H_2O_2), and hydrazine monohydrate ($N_2H_4{\cdot}H_2O$) were bought from Beijing Chemical Corporation (China). Nickel chloride hexahydrate ($NiCl_2{\cdot}6H_2O$), sodium dihydrogen phosphate ($NaH_2PO_4{\cdot}2H_2O$), sodium citrate dihydrate ($Na_3C_6H_5O_7{\cdot}2H_2O$), and salicylic acid ($C_7H_6O_3$) were obtained from Fuchen Chemical Reagent Co., Ltd. (Tianjin, China). Disodium phosphate dodecahydrate ($Na_2HPO_4{\cdot}12H_2O$) and sodium nitrite ($NaNO_2$) were purchased from Tianjin Aopusheng Chemical Sales Co., Ltd. (Tianjin, China). Titanium plate (TP) (thickness is 0.2 mm) was bought from Qingyuan Metal Materials Co., Ltd (Xingtai, China) and treated with 3 M HCl for 15 min before use. All reagents were analytical grade without further purification.

Preparation of Ni foam/TP: Ni foam/TP was synthesized through the dynamic hydrogen bubble template method. Using pre-treated TP as the working electrode, Ag/AgCl as the reference electrode, and Pt as the counter electrode. The plating solution consisted of 0.1 M $NiCl_2$ and 2.0 M NH_4Cl. The electrodeposition was performed at -2.0 A cm^{-2} for 120 s. Then, the Ni foam/TP was washed with ethanol and deionized water several times to completely remove residual ions of electrolyte, and dried at 40 °C.

Preparation of Ni film/TP: A prepared Ni foam/TP was transferred to a vial filled with ethanol and sonicated in an ultrasonic bath sonicator to remove the 3D foam structure. The Ni powders were obtained by evaporating the ethanol solvent at 40 °C. The dried Ni powders were then mixed with isopropanol and 5% Nafion, followed by sonicating for 30 min, and the prepared homogeneous ink was loaded on the TP (mass loading: 4.2 mg cm^{-2}).

Characterizations: X-ray diffraction (XRD) loaded a Cu Kα radiation target (40 kV,

30 mA) (SHIMADZU, Japan), scanning electron microscopy (SEM) with 5 kV acceleration voltage (ZEISS, Germany), transmission electron microscopy (TEM) with a Zeiss Libra 200FE, and X-ray photoelectron spectroscopy (XPS) (ESCALAB 250 Xi) were applied to study the composition and morphology of the prepared materials. Gas chromatography (GC) (Shimadzu GC-2014C) was used to detect gaseous products. Ultraviolet-visible spectrophotometer (UV-Vis) was applied to measure absorbance (SHIMADZU UV-1800).

Electrochemical measurements: Electrocatalytic tests were performed in a typical H-type cell separated by a Nafion 117 membrane using a CHI 660E electrochemical analyzer (CHI Instruments, Shanghai). The membrane was boiled in ultrapure water, H_2O_2 (5%) aqueous solution, and 0.5 M H_2SO_4 solution before use. Electrolyte solution (45 mL) was Ar-saturated 0.1 M PBS containing 0.1 M $NaNO_2$, using Ni foam/TP (0.5 × 0.5 cm^2) as the working electrode, graphite rod as the counter electrode and Ag/AgCl as the reference electrode, respectively. All the potentials in this work were transformed to reversible hydrogen electrode (RHE) via the following equation: E (RHE) = E (Ag/AgCl) + 0.059 × pH + 0.197 V. The linear sweep voltammetry (LSV) curves were tested from 0.1 to −1.0 V in 0.1 M PBS with and without 0.1 M NO_2^- at a scan rate of 5 mV s^{-1}. The double layer capacitance (C_{dl}) was estimated by plotting the $j = (j_a - j_c) / 2$ at 0.66 V against the scan rates, in which the j_a and j_c were the anodic and cathodic current density, respectively. The slope is that of the C_{dl} value. ECSA can be calculated according to the equation: ECSA = C_{dl} / 0.040 × A. A is the geometric area of the working electrode (0.25 cm^2). Electrochemical impedance spectra (EIS) were measured in a frequency domain ranging from 0.1 Hz to 10^5 Hz with 5 mV amplitude.

Determination of NH_3: The concentration of produced NH_3 was determined by the indophenol blue method.[1] The electrolytes of different potential and cycle tests were diluted 40 times, and the electrolytes of stability tests were diluted 200 times in H-cell. The electrolytes for different current density and stability tests were diluted 10 times and 100 times in Zn-NO_2^- battery, respectively. In detail, 2 mL of the diluted catholyte was mixed with 2 mL of 1 M NaOH coloring solution containing 5% salicylic acid and

5% sodium citrate. Then, 1 mL of 0.05 M NaClO and 0.2 mL of 1 wt% $C_5FeN_6Na_2O$ were added to the above solution. After standing for 2 h in the dark, the concentration of NH_3 was identified using UV-Vis spectroscopy. The concentration-absorbance curve was calibrated using a series of standard NH_4Cl solutions. The absorbance at 655 nm was measured to quantify the NH_3 concentration using standard NH_4Cl solutions ($y = 0.4265\ x + 0.0521$, $R^2 = 0.9994$).

Determination of N_2H_4: The N_2H_4 presented in the electrolyte was estimated by the Watt and Chrisp method.[2] The chromogenic reagent was obtained by mixing 5.99 g $C_9H_{11}NO$, 30 mL HCl and 300 mL C_2H_5OH. In detail, 1 mL of the catholyte was mixed with 1 mL of prepared color reagent and maintained for 15 min in the dark. The concentration of N_2H_4 was determined using the absorbance at a wavelength of 460 nm. The absorbance curves were calibrated using the standard N_2H_4 solution with a series of concentrations ($y = 0.6711\ x + 0.0645$, $R^2 = 0.9997$).

Determination of N_2 and H_2: N_2 and H_2 were quantified by GC.

Calculations of NH_3 FE and NH_3 yield:

$$FE = (6 \times F \times [NH_3] \times V) / (M_{NH3} \times Q) \times 100\%$$

$$NH_3\ yield = ([NH_3] \times V) / (M_{NH3} \times t \times A)$$

Where F is the Faraday constant (96485 C mol^{-1}), $[NH_3]$ is the measured NH_3 concentration, V is the volume of the cathodic reaction electrolyte (45 mL), M_{NH3} is the molecular mass of NH_3, Q is the total quantity of applied electricity, t is the reduction time (1 h), and A is the geometric area of the working electrode (0.25 cm^2). The partial current densities in Fig. 3a, one can multiply the average current density at each potential with the FE of each reduction product.

Zn-NO_2^- battery： In 0.1 M PBS with 0.1 M NO_2^-, the Ni foam/TP acted as the cathode to perform the NO_2^-RR. A polished Zn plate as the anode was placed in 1 M KOH and two electrolytes were separated by a bipolar membrane. During the battery discharge process, electrochemical NO_2^- reduction occurs on Ni foam/TP, and Zn converts to ZnO. The reactions on the anode and cathode were described as follows:

cathode: $NO_2^- + 6H_2O + 6e^- \rightarrow NH_4OH + 7OH^-$

anode: $3Zn + 6OH^- \rightarrow 3ZnO + 3H_2O + 6e^-$

overall: $3Zn + NO_2^- + 3H_2O \rightarrow 3ZnO + NH_4OH + OH^-$

Power density was determined using equation ($P = U \times I$) from the results of polarization data.

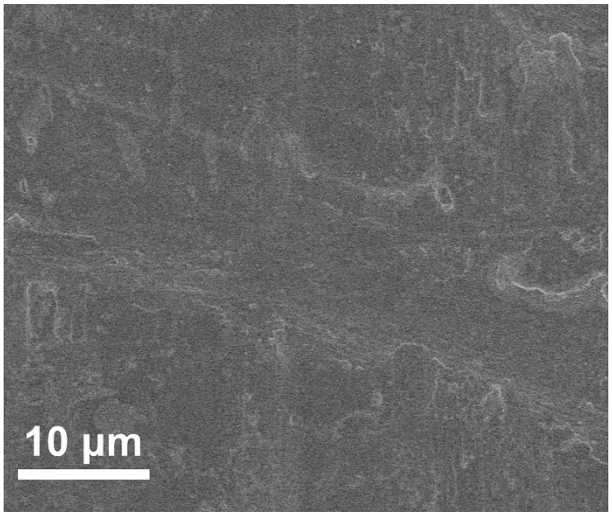

Fig. S1. SEM image of TP.

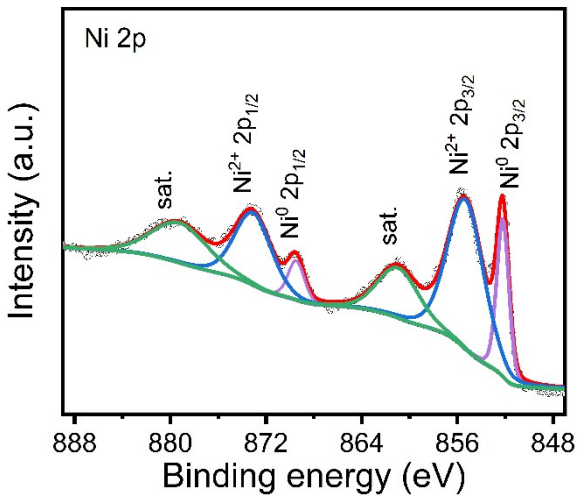

Fig. S2. XPS spectrum of Ni foam in the Ni 2p region.

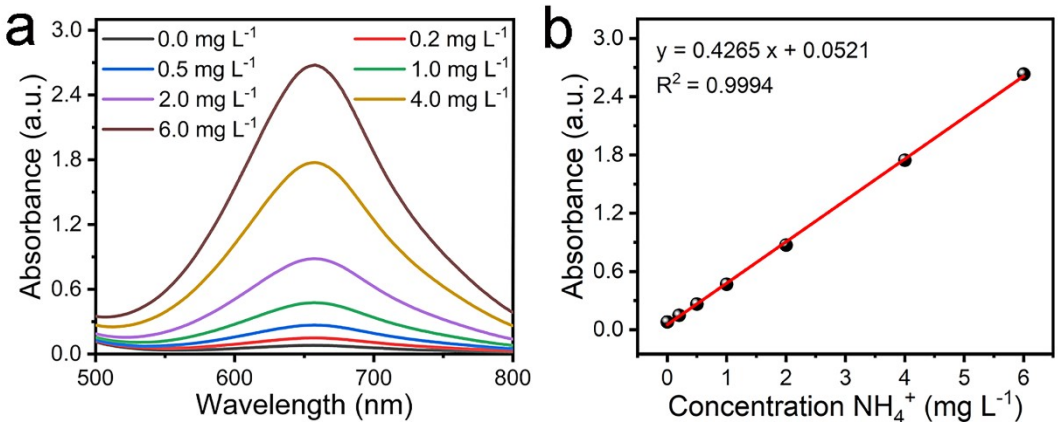

Fig. S3. (a) UV-Vis spectra of different NH_4^+ concentrations after incubation for 2 h. (b) Calibration curve used for calculating NH_4^+ concentration.

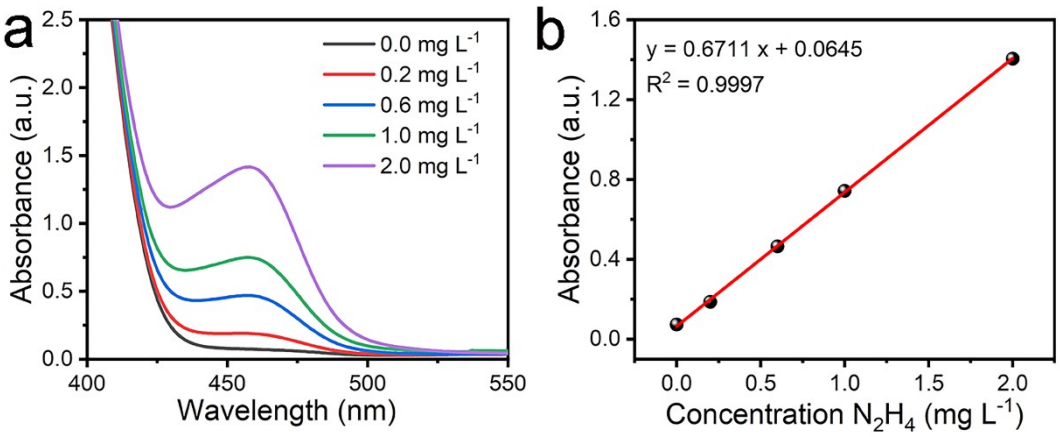

Fig. S4. (a) UV-Vis spectra of different N_2H_4 concentrations following 15 min of incubation. (b) Calibration curve applied to estimate N_2H_4 concentration.

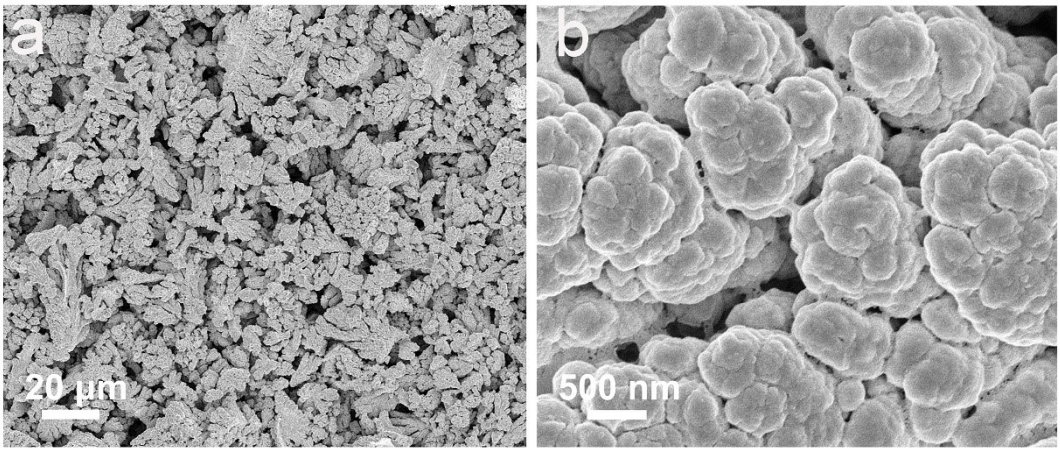

Fig. S5. SEM images of Ni film/TP.

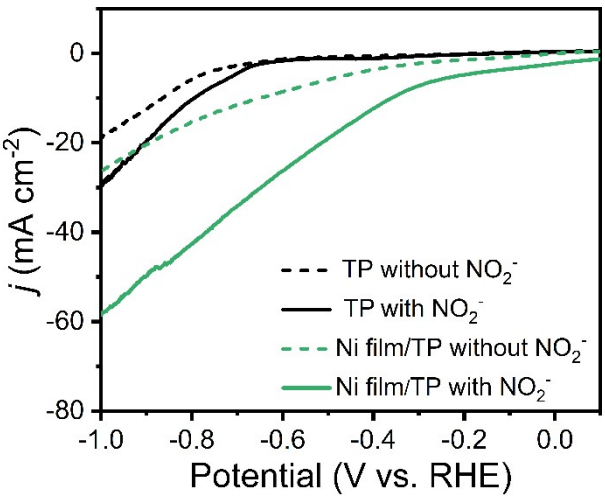

Fig. S6. LSV curves of Ni film/TP and TP in 0.1 M PBS with and without 0.1 M NO_2^-.

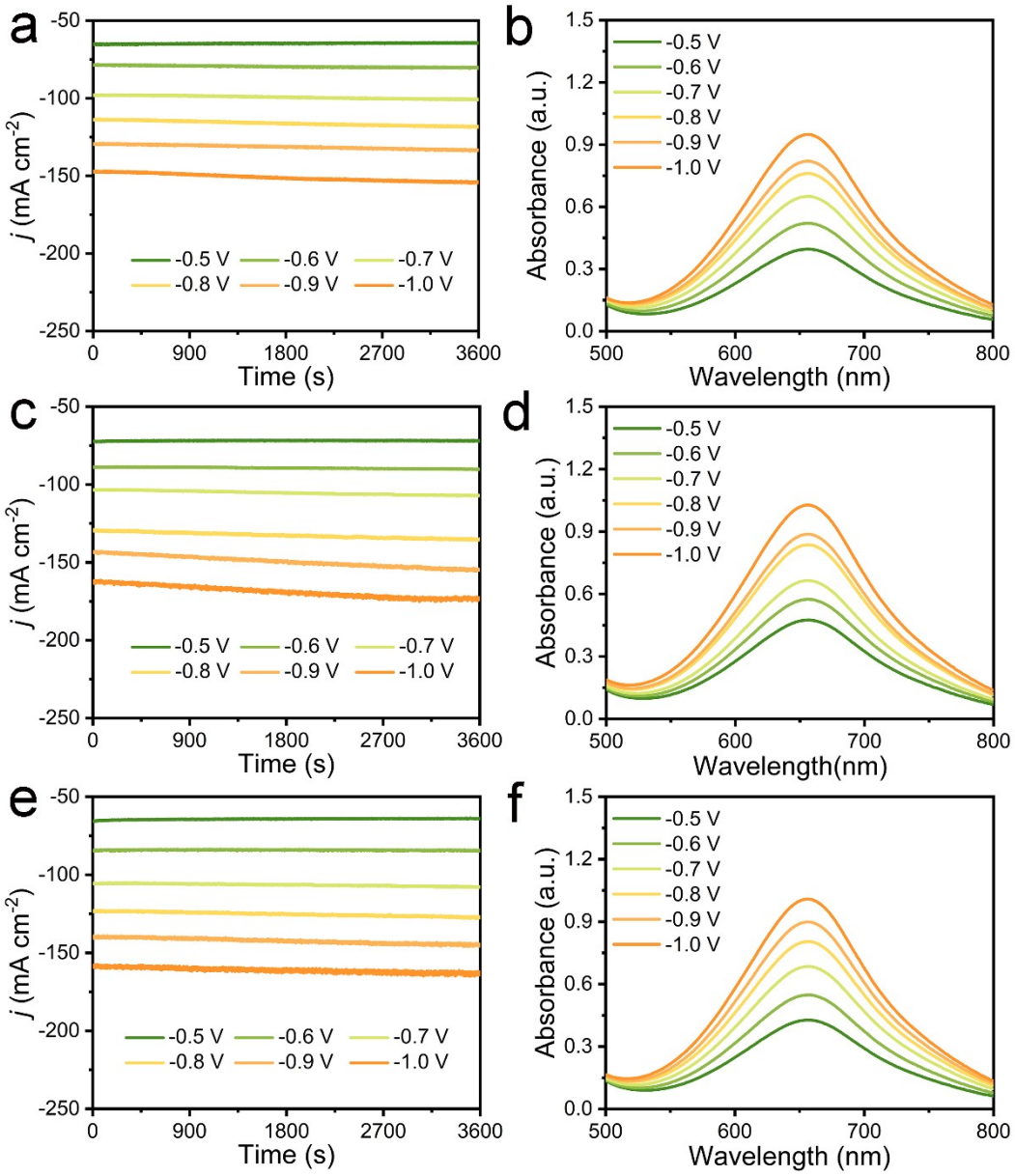

Fig. S7. (a, c, and e) CA curves and (b, d, and f) corresponding UV-Vis spectra of Ni foam/TP at various applied potentials.

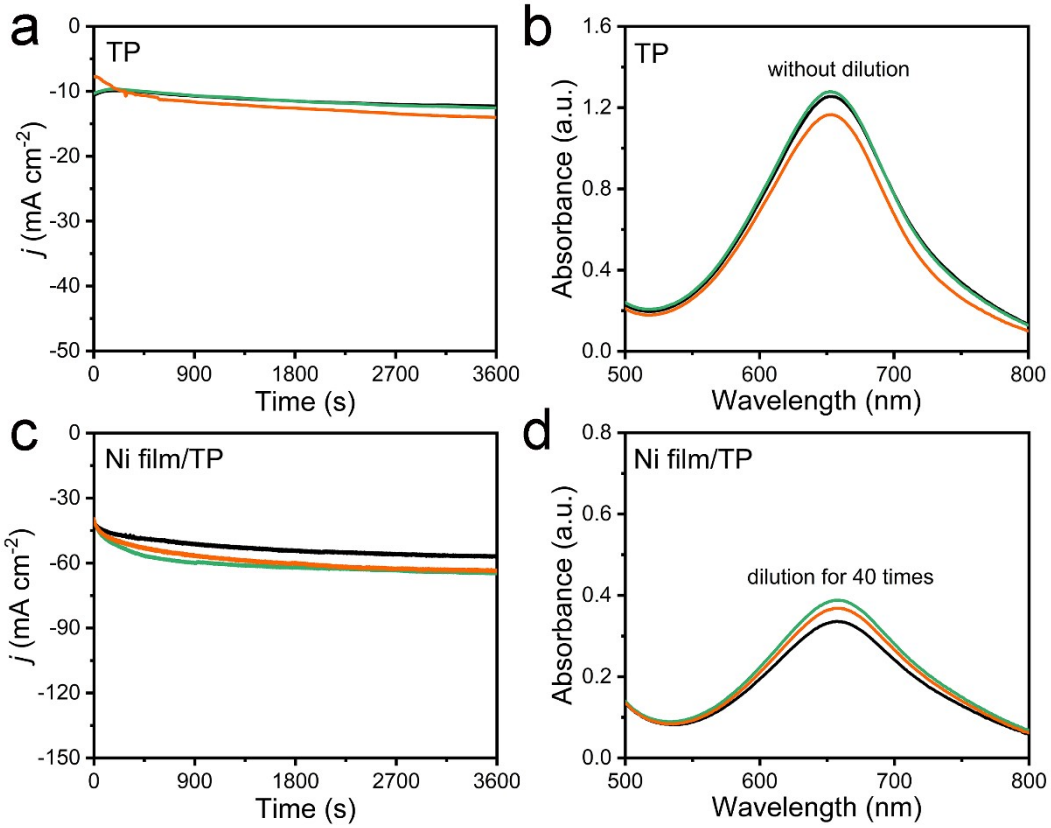

Fig. S8. (a) CA curves and (b) corresponding UV-Vis spectra of TP at −0.8 V. (c) CA curves and (b) corresponding UV-Vis spectra of Ni film/TP at −0.8 V.

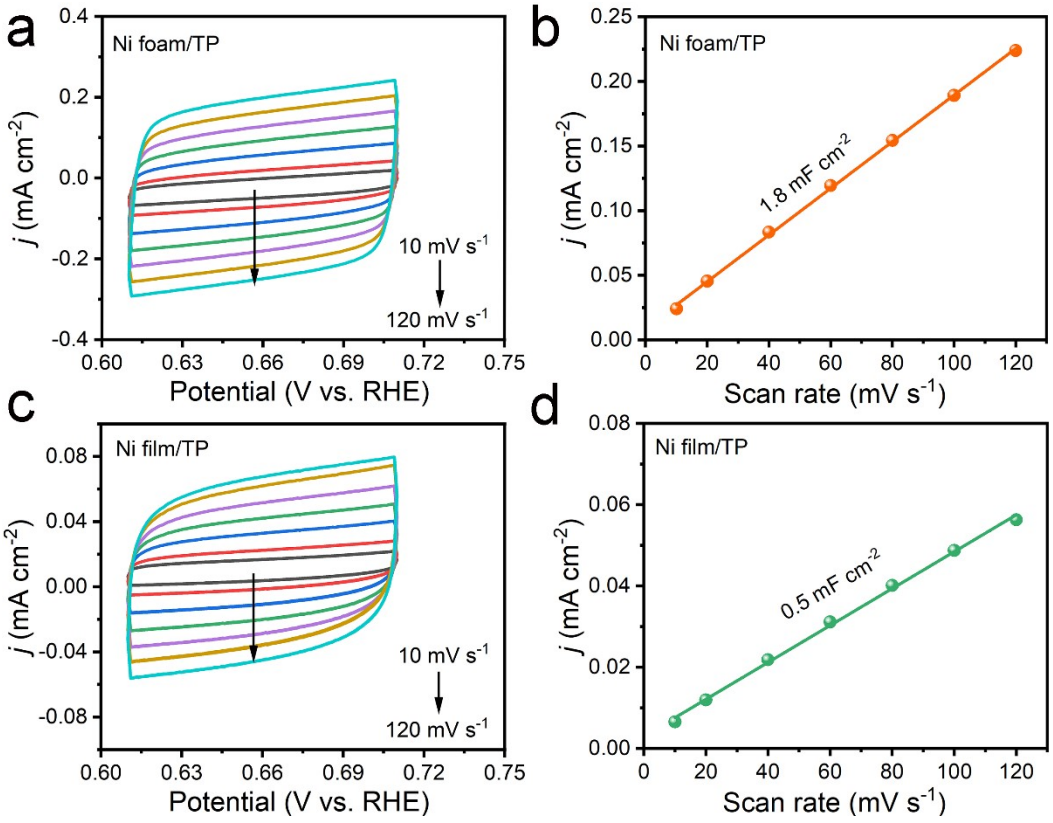

Fig. S9. CV curves for (a) Ni foam/TP and (c) Ni film/TP in the double layer region at scan rates of 10 to 120 mV s^{-1}. Capacitive currents as a function of scan rate for (b) Ni foam/TP and (d) Ni film/TP.

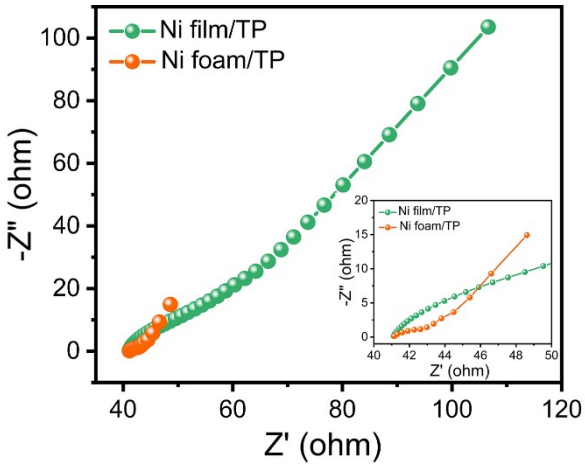

Fig. S10. EIS spectra of Ni foam/TP and Ni film/TP.

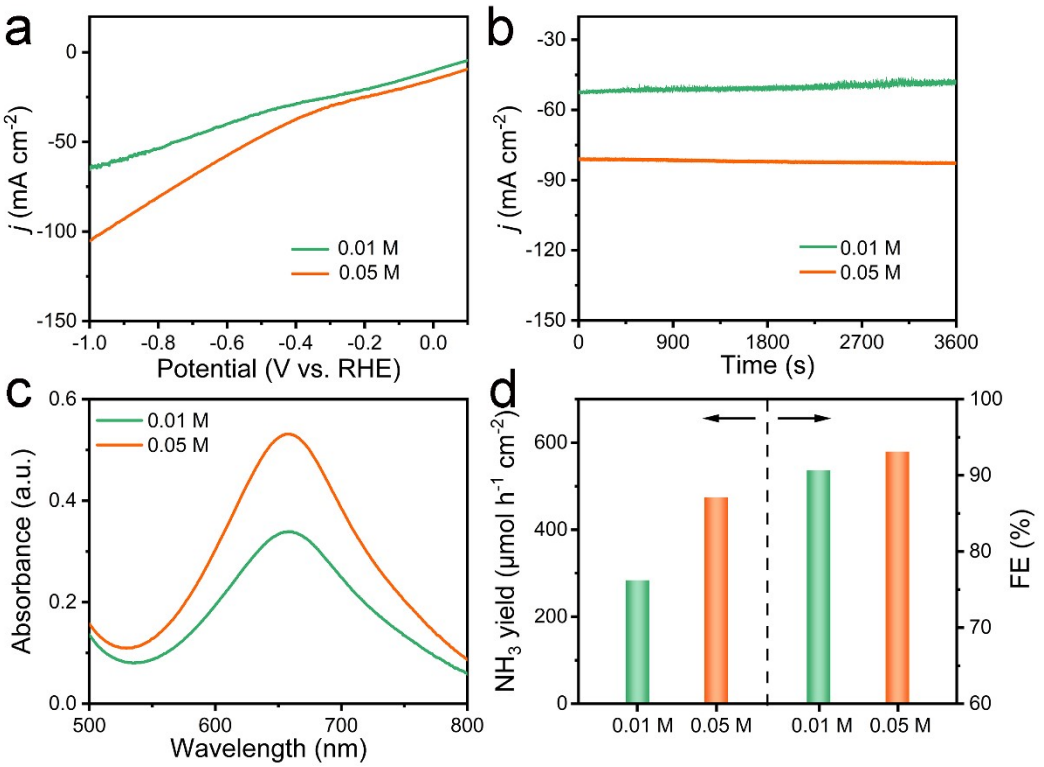

Fig. S11. (a) LSV curves, (b) CA curves, (c) corresponding UV-Vis spectra, and (d) NH_3 yields and FEs in 0.1 M PBS with different NO_2^- concentrations.

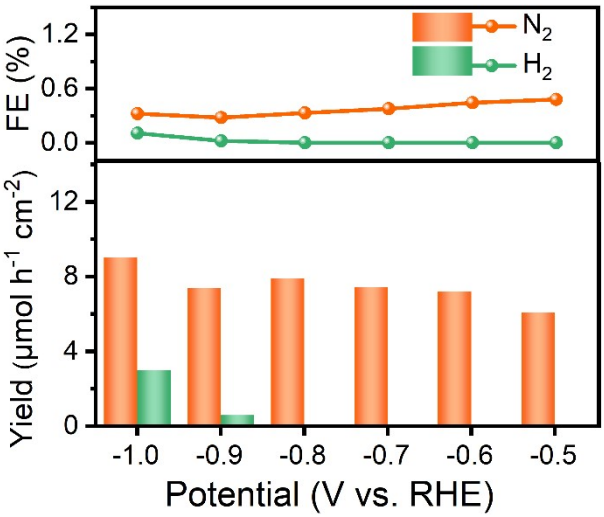

Fig. S12. FEs and yields of H_2 and N_2 for Ni foam/TP at different potentials detected by GC.

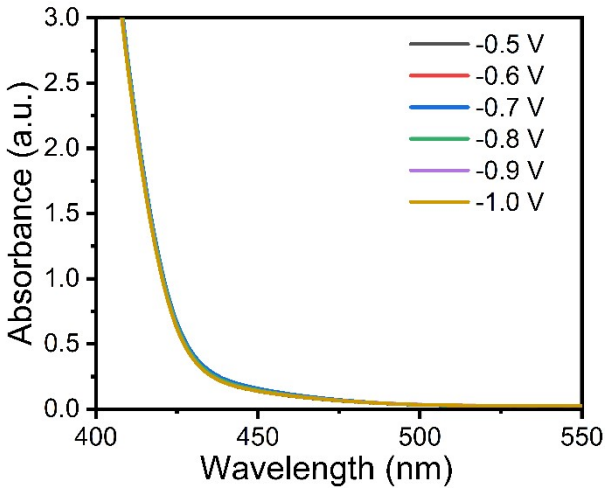

Fig. S13. UV-Vis spectra of electrogenerated N_2H_4 for Ni foam/TP at different potentials.

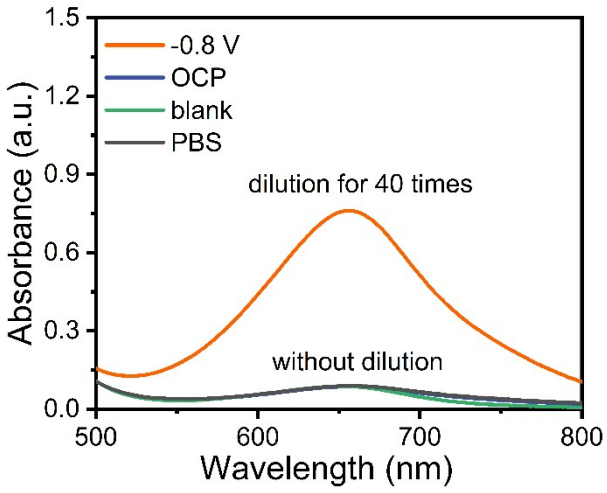

Fig. S14. (a) UV-Vis spectra of Ni foam/TP for the NO_2^-RR at different conditions.

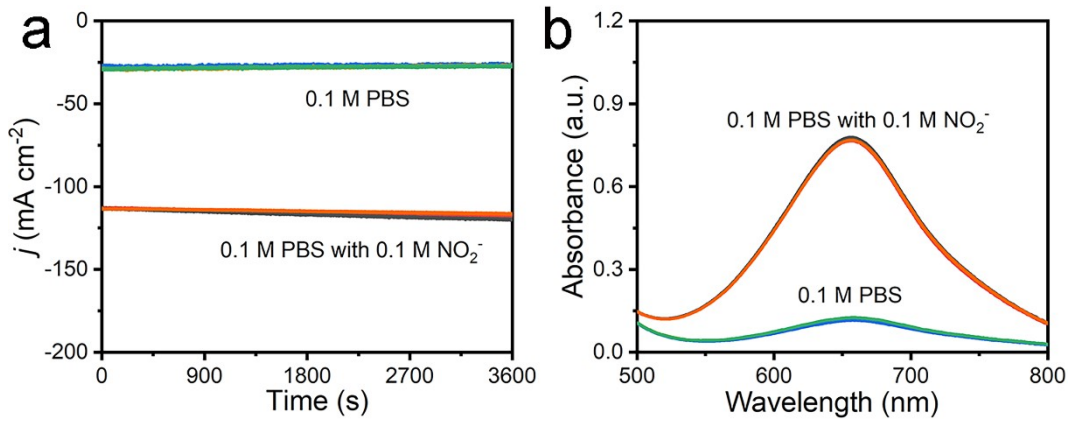

Fig. S15. (a) CA curves and (b) corresponding UV-Vis spectra of Ni foam/TP for alternating cycle tests in 0.1 M PBS with and without 0.1 M NO_2^-.

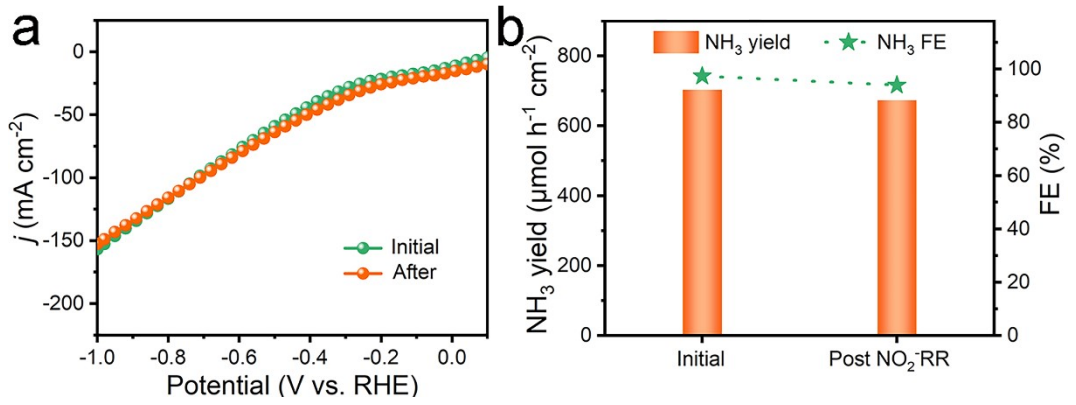

Fig. S16. (a) LSV curves of Ni foam/TP before and after 12-h electrolysis test. (b) NH_3 yields and FEs at −0.80 V for 1 h of initial Ni foam/TP and Ni foam/TP tested for 12 h.

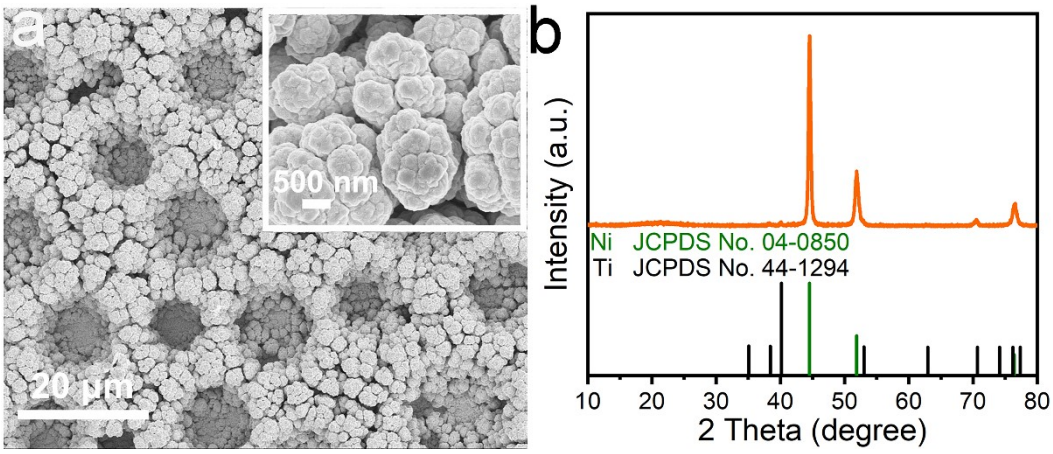

Fig. S17. (a) SEM images and (b) XRD pattern of Ni foam/TP after stability test.

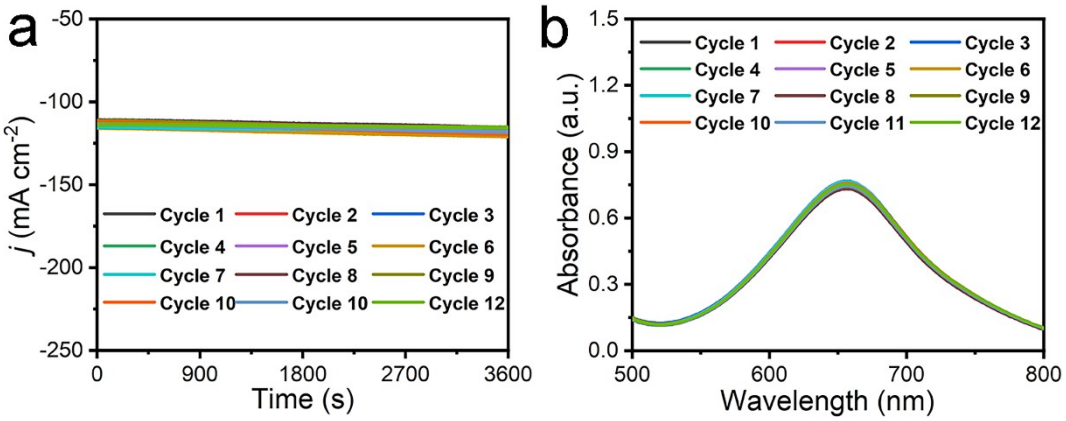

Fig. S18. (a) CA curves and (b) corresponding UV-Vis spectra of Ni foam/TP during recycling tests at −0.8 V.

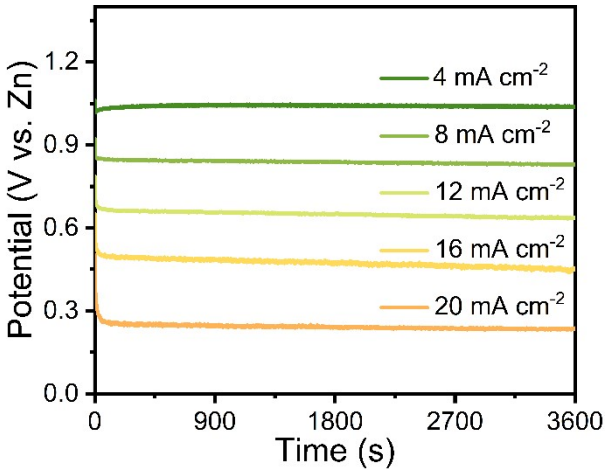

Fig. S19. (a) Discharge curves of Ni foam/TP-based Zn-NO_2^- battery at various current densities per 1 h.

Table S1. Comparison of the C_{dl} and ECSA values of Ni foam/TP and Ni film/TP.

	C_{dl} (mF cm^{-2})	**ECSA (cm^2)**
Ni foam/TP	1.8	11.3
Ni film/TP	0.5	3.1

Table S2. Comparison of the catalytic performances of Ni foam/TP with other reported NO_2^-RR electrocatalysts.

Catalyst	Electrolyte	FE (%) @Potential (V vs. RHE)	NH_3 yield (μmol h^{-1} cm^{-2}) @Potential (V vs. RHE)	Ref.
Ni foam/TP	0.1 M PBS (0.1 M NO_2^-)	97.4@−0.8	889.6@−1.0	This work
Ag@NiO/CC	0.1 M NaOH (0.1 M NO_2^-)	97.7@−0.4	338.3@−0.7	3
Ru–Cu NW/CF	0.1 M PBS (500 ppm NO_2^-)	94.1@−0.6	732.0@−0.6	4
Ru–TiO_2/TP	0.1 M NaOH (0.1 M NO_2^-)	98.9@−0.5	1560.0@−0.7	5
Ni-NSA-VNi	0.2 M Na_2SO_4 (200 ppm NO_2^-)	88.9@−0.54	236.0@−0.54	6
NiS_2@TiO_2/TM	0.1 M NaOH (0.1 M NO_2^-)	92.1@−0.5	591.9@−0.6	7
Ni@JBC	0.1 M NaOH (0.1 M NO_2^-)	83.4@−0.5	48.5@−0.5	8
Ni–TiO_2/TP	0.1 M NaOH (0.1 M NO_2^-)	94.9@−0.5	727.0@−0.7	9
Ni@MDC	0.1 M NaOH (0.1 M NO_2^-)	65.4@−0.8	74.1@−0.8	10
CoB@TiO_2/TP	0.1 M Na_2SO_4 (400 ppm NO_2^-)	95.2@−0.7	293.0@−0.9	11
Cu_3P NA/CF	0.1 M PBS (0.1 M NO_2^-)	91.2@−0.5	95.7@−0.5	12
Fe_2P/AS/CP	0.1 M KOH (0.1 M NO_2^-)	96.8@−0.5	318.9@−0.6	13
CoP NA/TM	0.1 M PBS (500 ppm NO_2^-)	90.0@−0.2	133.0@−0.2	14
V–TiO_2/TP	0.1 M NaOH (0.1 M NO_2^-)	93.2@−0.6	540.8@−0.7	15

Table S3. Comparison of NH_3 yield and power density of our battery with other reported Zn-NO_x and Zn-N_2 batteries.

Catalyst	Battery type	NH_3 yield (μmol h^{-1} cm^{-2})	Power density (mW cm^{-2})	Ref.
Ni foam/TP	Zn-NO_2^-	110.2	6.2	This work
C-$NiWO_4$/NF	Zn-NO_2^-	129.1	5.55	16
C@Co_3O_4	Zn-NO_2^-	47.2	6.03	17
CoP@TiO_2/TP	Zn-NO_2^-	42.0	1.24	18
Fe/Ni_2P	Zn-NO_3^-	22.6	3.25	19
CoNi-Vp	Zn-NO_3^-	12.2	1.05	20
vCo-Co_3O_4/CC	Zn-NO_3^-	109.9	8.1	21
NiO/TM	Zn-NO	13.4	0.88	22
Bi@C	Zn-NO	20.9	2.35	23
OV-Ti_2O_3	Zn-N_2	0.025	1.02	24
CoPi/HSNPC	Zn-N_2	0.97	0.33	25

References

1 D. Zhu, L. Zhang, R. E. Ruther and R. J. Hamers, *Nat. Mater.*, 2013, **12**, 836–841.

2 G. W. Watt and J. D. Chrisp, *Anal. Chem.*, 1952, **24**, 2006–2008.

3 Q. Liu, G. Wen, D. Zhao, L. Xie, S. Sun, L. Zhang, Y. Luo, A. Ali Alshehri, M. S. Hamdy, Q. Kong and X. Sun, *J. Colloid Interface Sci.*, 2022, **623**, 513–519.

4 N. Q. Tran, L. T. Duy, D. C. Truong, B. T. Nguyen Le, B. T. Phan, Y. Cho, X. Liu and H. Lee, *Chem. Commun.*, 2022, **58**, 5257–5260.

5 Y. Ren, Q. Zhou, J. Li, X. He, X. Fan, Y. Fu, X. Fang, Z. Cai, S. Sun, M. S. Hamdy, J. Zhang, F. Gong, Y. Liu and X. Sun, *J. Colloid Interface Sci.*, 2023, **645**, 806–812.

6 C. Wang, W. Zhou, Z. Sun, Y. Wang, B. Zhang and Y. Yu, *J. Mater. Chem. A*, 2021, **9**, 239–243.

7 X. He, L. Hu, L. Xie, Z. Li, J. Chen, X. Li, J. Li, L. Zhang, X. Fang, D. Zheng, S. Sun, J. Zhang, A. Ali Alshehri, Y. Luo, Q. Liu, Y. Wang and X. Sun, *J. Colloid Interface Sci.*, 2023, **634**, 86–92.

8 X. Li, Z. Li, L. Zhang, D. Zhao, J. Li, S. Sun, L. Xie, Q. Liu, A. A. Alshehri, Y. Luo, Y. Liao, Q. Kong and X. Sun, *Nanoscale*, 2022, **14**, 13073–13077.

9 Z. Cai, C. Ma, D. Zhao, X. Fan, R. Li, L. Zhang, J. Li, X. He, Y. Luo, D. Zheng, Y. Wang, B. Ying, S. Sun, J. Xu, Q. Lu and X. Sun, *Mater. Today Energy*, 2023, **31**, 101220.

10 X. He, X. Li, X. Fan, J. Li, D. Zhao, L. Zhang, S. Sun, Y. Luo, D. Zheng, L. Xie, A. M. Asiri, Q. Liu and X. Sun, *ACS Appl. Nano Mater.*, 2022, **5**, 14246–14250.

11 L. Hu, D. Zhao, C. Liu, Y. Liang, D. Zheng, S. Sun, Q. Li, Q. Liu, Y. Luo, Y. Liao, L. Xie and X. Sun, *Inorg. Chem. Front.*, 2022, **9**, 6075–6079.

12 J. Liang, B. Deng, Q. Liu, G. Wen, Q. Liu, T. Li, Y. Luo, A. A. Alshehri, K. A. Alzahrani, D. Ma and X. Sun, *Green Chem.*, 2021, **23**, 5487–5493.

13 J. Hu, T. Zhao, H. Zhang, X. Li, A. Shi, X. Li, Q. Wang and G. Hu, *Surf. Interfaces*, 2023, **38**, 102818.

14 G. Wen, J. Liang, Q. Liu, T. Li, X. An, F. Zhang, A. A. Alshehri, K. A. Alzahrani,

Y. Luo, Q. Kong and X. Sun, *Nano Res.*, 2022, **15**, 972–977.

15 H. Wang, F. Zhang, M. Jin, D. Zhao, X. Fan, Z. Li, Y. Luo, D. Zheng, T. Li, Y. Wang, B. Ying, S. Sun, Q. Liu, X. Liu and X. Sun, *Mater. Today Phys.*, 2023, **30**, 100944.

16 H. Qiu, Q. Chen, J. Zhang, X. An, Q. Liu, L. Xie, W. Yao, X. Sun and Q. Kong, *Inorg. Chem. Front.*, 2023, **10**, 3909–3915.

17 R. Zhang, S. Zhang, Y. Guo, C. Li, J. Liu, Z. Huang, Y. Zhao, Y. Li and C. Zhi, *Energy Environ. Sci.*, 2022, **15**, 3024–3032.

18 X. He, Z. Li, J. Yao, K. Dong, X. Li, L. Hu, S. Sun, Z. Cai, D. Zheng, Y. Luo, B. Ying, M. S. Hamdy, L. Xie, Q. Liu and X. Sun, *iScience*, 2023, **26**, 107100.

19 R. Zhang, Y. Guo, S. Zhang, D. Chen, Y. Zhao, Z. Huang, L. Ma, P. Li, Q. Yang, G. Liang and C. Zhi, *Adv. Energy Mater.*, 2022, **12**, 2103872.

20 Y. Gao, K. Wang, C. Xu, H. Fang, H. Yu, H. Zhang, S. Li, C. Li and F. Huang, *Appl. Catal., B*, 2023, **330**, 122627.

21 Z. Deng, C. Ma, Z. Li, Y. Luo, L. Zhang, S. Sun, Q. Liu, J. Du, Q. Lu, B. Zheng and X. Sun, *Acs Appl. Mater. Interfaces*, 2022, **14**, 46595–46602.

22 P. Liu, J. Liang, J. Wang, L. Zhang, J. Li, L. Yue, Y. Ren, T. Li, Y. Luo, N. Li, B. Tang, Q. Liu, A. M. Asiri, Q. Kong and X. Sun, *Chem. Commun.*, 2021, **57**, 13562–13565.

23 Q. Liu, Y. Lin, L. Yue, J. Liang, L. Zhang, T. Li, Y. Luo, M. Liu, J. You, A. A. Alshehri, Q. Kong and X. Sun, *Nano Res.*, 2022, **15**, 5032–5037.

24 H.-j. Chen, Z.-q. Xu, S. Sun, Y. Luo, Q. Liu, M. S. Hamdy, Z.-s. Feng, X. Sun and Y. Wang, *Inorg. Chem. Front.*, 2022, **9**, 4608–4613.

25 J.-T. Ren, L. Chen, Y. Liu and Z.-Y. Yuan, *J. Mater. Chem. A*, 2021, **9**, 11370–11380.